Check for updates

Received: 10 June 2021 | Revised: 3 September 2021 | Accepted: 8 September 2021

DOI: 10.1002/hyp.14375

RESEARCH ARTICLE

WILEY

Fluvial suspended sediment transfer and lacustrine sedimentation of recent flood turbidites in proglacial Eklutna Lake, western Chugach Mountains, Alaska

Erik Schiefer[1] | Jason Geck[2] | Johnse S. Ostman[2] | Nicholas P. McKay[3] | Nore Praet[4] | Michael G. Loso[5] | Darrell S. Kaufman[3]

[1]Department of Geography, Planning & Recreation, Northern Arizona University, Flagstaff, Arizona, USA

[2]Institute of Culture and Environment, Alaska Pacific University, Anchorage, Alaska, USA

[3]School of Earth & Sustainability, Northern Arizona University, Flagstaff, Arizona, USA

[4]Renard Centre of Marine Geology, Ghent University, Ghent, Belgium

[5]National Park Service, Wrangell-St. Elias National Park and Preserve, Copper Center, Alaska, USA

Correspondence
Erik Schiefer, Northern Arizona University, Department of Geography, Planning & Recreation, Flagstaff, AZ, USA.
Email: erik.schiefer@nau.edu

Present address
Nore Praet, Flanders Marine Institute, Ostend, Belgium

Funding information
Office of Polar Programs, Grant/Award Number: ARC-1418000; Alaska Space Grant Program

Abstract

Suspended sediment delivery and deposition in proglacial lakes is generally sensitive to a wide range of hydrometeorologic and geomorphic controls. High discharge conditions are of particular importance in many glaciolacustrine records, with individual floods potentially recorded as distinctive turbidites. We used an extensive network of surface sediment cores and hydroclimatic monitoring data to analyse recent flood turbidites and associated sediment transfer controls over instrumental periods at Eklutna Lake, western Chugach Mountains, Alaska. Close to a decade of fluvial data from primary catchment tributaries show a dominating influence of discharge on sediment delivery, with various interconnections with other related hydroclimatic controls. Multivariate fluvial models highlight and help quantify some complexities in sediment transfer, including intra-annual variations, meteorological controls, and the influence of subcatchment glacierization. Sediments deposited in Eklutna Lake during the last half century are discontinuously varved and contain multiple distinctive turbidites. Over a 30-year period of stratigraphic calibration, we correlate the four thickest flood turbidites (1989, 1995, 2006, and 2012) to specific regional storms. The studied turbidites correlate with late-summer and early-autumn rainstorms with a magnitude of relatively instantaneous sedimentation 3–15 times greater than annual background accumulation. Our network of sediment core data captured the broad extent and sediment variability among the study turbidites and background sediment yield. Within-lake spatial modelling of deposition quantifies variable rates of downlake thinning and sediment focusing effects, and highlights especially large differences between the thickest flood turbidites and background sedimentation. This we primarily relate to strongly contrasting dispersion processes controlled by inflow current strength and turbidity. Sediment delivery is of interest for this catchment because of reservoir and water supply operations. Furthermore, although smaller floods may not be consistently represented, the lake likely contains a valuable proxy record of regional flooding proximal to major population centers of south-central Alaska including Anchorage.

KEYWORDS
Eklutna Lake, flood turbidites, fluvial suspended sediment, lake sediment, sediment yield

 © 2021 John Wiley & Sons Ltd.

1 | INTRODUCTION

Lake sediments can contain valuable records of catchment floods, often stored in lacustrine deposits as distinctive flood turbidites (Gilli et al., 2013; Schillereff et al., 2014). Turbidites in proglacial lakes receiving runoff from alpine glaciers have been linked to floods generated by heavy precipitation (e.g., Amann et al., 2015; Ekblom Johansson et al., 2020; Fouinat et al., 2017; Roop et al., 2016), snowmelt (e.g., Menounos & Clague, 2008; Røthe et al., 2018; Schiefer, 2006), and jökulhlaups (e.g., Boes et al., 2018; Jacquet et al., 2017), in addition to other confounding geomorphic events such as earthquakes (e.g., Praet et al., 2017; Wilhelm et al., 2016) and landslides (e.g., Heideman et al., 2018; Sletten et al., 2003). This study investigates recent sediment transfer processes and flood turbidite deposition in Eklutna Lake, a managed reservoir and recreation site in the Chugach Mountains proximal to major population centers of south-central Alaska, including the Municipality of Anchorage and lower Matanuska-Susitna valley.

Previous works have identified and described turbidites in the sedimentary record of Eklutna Lake. Flood turbidites are mentioned in Praet et al. (2017) although the focus of that study was earthquake-generated 'megaturbidites' with multi-century recurrence intervals (e.g., 1964 M_W 9.2). In a study of varve formation processes during the past three centuries in Eklutna Lake, Boes et al. (2018) describe in detail the presence of coarse-grained turbidites likely related to episodes of high sediment discharge during floods. These turbidites, which become more frequent since the nineteenth century, were associated with rain events and/or intense snow and ice melt. Boes et al. (2018) provide a detailed stratigraphic analysis of the Eklutna Lake clastic varves and investigates large-scale catchment geomorphology and hydroclimatic controls of sediment transfer. They also establish exceptional chronological control of sedimentation for most of the last century using radiometric dating, varve counting, event stratigraphy and tephrochronology, and they describe two recent flood turbidites occurring in 1989 and 1995. More recent work has examined how to differentiate between known earthquake-triggered turbidites (1964 M_W 9.2 and 2018 M_W 7.1) and flood-triggered turbidites (1989 and 1995) using a variety of sedimentary characteristics, including within-lake spatial deposition patterns, to facilitate prehistoric earthquake and flood reconstructions (Praet et al., 2020; Van Daele et al., 2020; Vandekerkhove et al., 2020).

Expanding on previous research, the objectives of this study are to: (1) Use available fluvial and meteorological data to develop multivariate sediment rating curves for primary tributaries to Eklutna Lake to gain insight into hydroclimatic controls of sediment delivery; (2) Examine and statistically model the spatial signatures of recent flood turbidites over a greater range of sediment delivery magnitudes to better understand variability in depositional patterns; and (3) Assess the potential for calibrating the flood turbidite record from Eklutna Lake sediments for flood proxy development in the western Chugach Mountains of south-central Alaska.

2 | STUDY AREA

Eklutna Lake (61.38°N 149.04°W; 265 m asl) is situated in the western Chugach Mountains about 40 km northeast of Anchorage, in Chugach State Park. The lake averages 1.4 km wide and 10.5 km long within the Eklutna River valley glacial trough, dammed by a recessional moraine of the Pleistocene Eklutna Glacier (Brabets, 1993). Bathymetric mapping (Figure 1(a)) shows two major lake basins with maximum depths of about 60 and 50 m, herein referred to as the proximal (southeast) and distal (northwest) basins, respectively, based on location relative to dominant lake inflow at the southeast end. The basins are separated by a submerged end moraine with further lateral confinement at that location by side tributary fans. The Eklutna Lake natural dam threshold was first modified in 1928 for hydroelectric development, and then more substantially modified in 1964 to repair earthquake damage, cumulatively raising the reservoir level by over 5 m. The Municipality of Anchorage draws lake water for power generation and water supply, with diversion control now dominating the amplitude and timing of annual water level fluctuations. Mid-lake temperature-turbidity profiles show thermal stratification with an epilimnic base around 5–10 m and evidence of turbid interfows centered around 10–20 m water depths during summer, non-flood conditions 1982–1988 (Brabets, 1993; R&M Consultants, 1986) and 2015–2018 (J. Geck, unpublished data). Eklutna Lake sediments comprise silt-clay clastic varves of varying quality and thickness, interbedded by thicker and coarser, distinctive turbidites. The high-resolution, high-certainty event chronology developed for the lake includes 1989 and 1995 flood turbidites (Boes et al., 2018). Multiple years of repeat coring confirm the annual character of the couplets and unambiguously link two more minor turbidites to a high-discharge 2017 event and a 2018 earthquake (Van Daele et al., 2020). From 1985 to 1987, bedload of mostly coarse sand and gravel constituted 10%–18% of total sediment transport to the lake (Brabets, 1993).

The Eklutna Lake catchment (311 km^2) is dominated by two main sub-catchment tributaries, West Fork Eklutna Creek and East Fork Eklutna Creek (Figure 1(b)), herein referred to as West Fork (WF) and East Fork (EF), respectively. These two creeks currently merge 0.8 km up-valley from the major inflow delta at the southeast end of the lake (Figure 1(c) and (d)). Smaller side tributaries, from which overall sediment load is relatively minimal, account for the remainder of lake inflow (Brabets, 1993). Catchment bedrock consists of structurally complex and variably metamorphosed sedimentary and igneous rocks (Wilson & Hults, 2012). Alluvium deposits are dominant around the lake and colluvium mantles much of the lower mountain slopes. Extensive glaciofluvial deposits occur along EF and WF downstream of large catchment glaciers. Upland cirques contain glacial deposits and exposed bedrock dominates highest elevations. Glacier coverage of the lake catchment was 13% in 2015 with numerous glaciers of various sizes, including a series of small cirque glaciers in the EF catchment (19% glacier cover), and the 12 km long Eklutna Glacier of the WF catchment (48% glacier cover) (Sass et al., 2017). Some glacially sculpted peaks and ridges along the southern half of the upper catchment divide exceed 2000 m asl, including the highest peak of Chugach

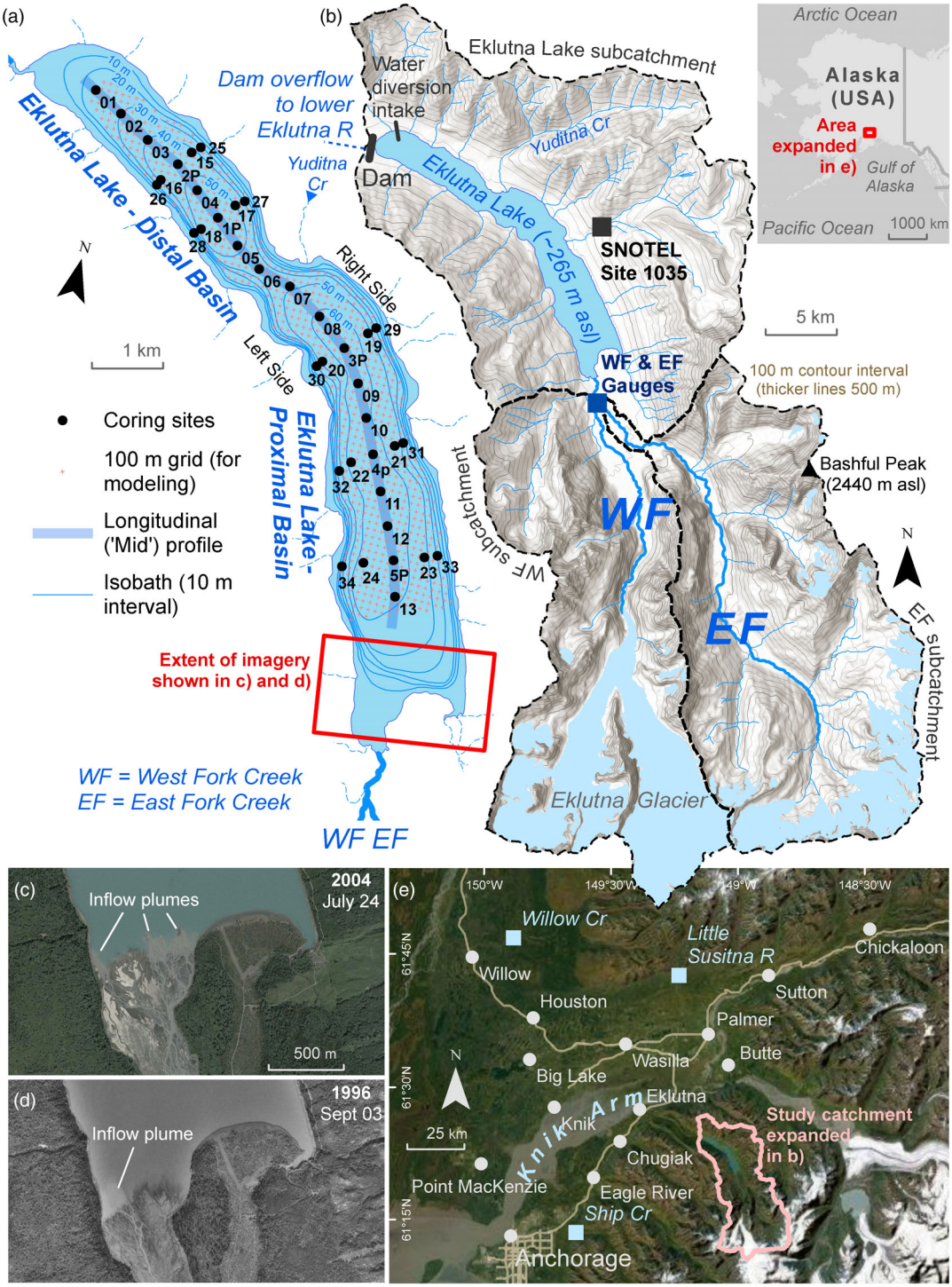


FIGURE 1 Study maps: (a) Eklutna Lake bathymetry, inflows, and coring sites; (b) upper Eklutna (above dam) catchment topography, subcatchment divides, and hydroclimatic stations; (c) inflow plumes visible in 24-July-2004 USGS air photos; (d) inflow plumes visible in 03-Sept-1996 USGS air photos; (e) study region map with base satellite imagery, communities, highways, and other stream gauges analysed

State Park, Bashful Peak (2440 m asl). Dam overflow drains northward to Knik Arm, which joins the Gulf of Alaska through Cook Inlet. Forest cover (white spruce, birch and aspen) is present around the lake and in the lower valley bottoms, but the majority of the catchment lies above tree line.

Meteorological data from within the Eklutna Lake catchment is available for a mid-elevation site since 2002 (US Natural Resources Conservation Service – SNOTEL Site 1035, 640 m asl) (Figure 1(b)), showing mean monthly temperatures ranging from −6.9°C (January) to 10.6°C (July), and mean annual precipitation of 521 mm with peak precipitation months in late summer to early autumn. Stream gauging was established on lower reaches of EF (101 km^2) and WF (66 km^2) in 2009 for ongoing discharge and sediment transport monitoring (Ostman et al., in progress). Hydrographs exhibit significant year-to-

year variability in runoff timing and total volume, but with similar seasonal trends of discharge initiated by early onset melt runoff in May and spring freshet flows culminating in June or early July. During higher summer melt rates, diurnal fluctuations are apparent with peaks occurring at about 20:00 and 16:00 for EF and WF, respectively. Seasonal peak discharges occurring in late July or early August coincide with rain events and/or maximal glacier melt. The late-season falling hydrograph limbs are often interrupted by significant late-summer and early-autumn precipitation events until freeze-up and ice effects begin in October. Median peak discharges (2009–2018) for EF and WF are approximately 20 and 30 $m^3\ s^{-1}$, respectively. Turbidity and sediment concentrations correlate with discharge, and are typically higher in WF than in EF. Data from USGS gauges around the relatively populated surrounding areas of Anchorage and the lower Matanuska-Susitna basin provide regional discharge data for similarly sized catchments (Figure 1(e)).

3 | METHODS

3.1 | Fluvial sediment transfer

We use Eklutna catchment discharge data for WF and EF derived by standard USGS stream gauging and rating curve methods (Rantz, 1982) to construct continuous discharge (Ostman et al., in progress). ISCO (model 6700) automatic pump water sampling at the gauge sites was initiated in 2015 for suspended sediment monitoring with the intention of continuing data collection for several years. The ISCOs collected two 500 mL water samples daily at 08:00 and 20:00 to capture a large proportion of observed diurnal ranges. Isokinetic depth-integrated water samples were also infrequently collected with US-DH48 or -DH81 (low water) samplers to check consistency of ISCO sediment measures and to add data at intermediate times. Vacuum filtering of the water samples with pre-weighed filters (0.45 μm) was used to determine suspended sediment concentrations (SSCs; $mg\ L^{-1}$). Result comparisons supported the accuracy of the automatic sampling consistent with previous studies (e.g., Gurnell et al., 1992; Richards & Moore, 2003). Hourly turbidity data measured in Nephelometric Turbidity Units (NTU) was initiated earlier in 2008 for long-term sediment transfer monitoring using Campbell Scientific meters (models CR800 and CR1000). Finally, for sediment rating curve modelling, we also used meteorological data processed by Ostman (in progress), based on expansion and filtering of the SNOTEL temperature and precipitation records. For estimating fluvial sediment loads and sediment rating curve modelling, we aimed to span the full months of May through October as the catchment open-channel season, which we expect captures the vast majority of annual sediment delivery.

We followed the approach of Schiefer et al. (2017) to develop SSC- and NTU-based sediment rating curve models for WF and EF. This approach was a modification to that of Hodgkins (1999), involving exhaustive candidate model selection including pairwise interaction effects and trigonometric variable addition to capture diurnal variability. A total of eight variables were entered into our candidate model testing, including discharge (Q; $m^3\ s^{-1}$), Julian day number (*Julian*; days), hourly rate of change in Q (ΔQ; $m^3\ s^{-1}$), time since Q was exceeded (*Qe*; days, up to a maximum of 30 days), average temperature ($temp_{24hrs}$; °C) and total rainfall ($rain_{24hrs}$; mm) during previous 24 h periods, and the cosine and sine of the decimal hour time of day $\times\ 15^\circ\ h^{-1}$ (cos_{hr} and sin_{hr}), emphasizing midnight versus noon and early morning (6:00) versus late afternoon (18:00) differences, respectively. Preliminary model assessments included *Qe* periods greater than 30 days and climate data averaged over durations shorter than 24 h, but these predictor variants did not improve model fits. The NTU time series were median filtered (3 h window) to reduce signal noise. The dependent SSC and NTU variables, and Q predictor variables were $\log_e$ transformed to achieve approximate normality of model residuals. We used the R package *glmulti* (Calcagno & de Mazancourt, 2010) for exhaustive model fitting, but followed that with a stepwise backward approach to reduce overfitting by only retaining predictors if they lower the model Akaike's information criterion (AIC) by at least two (Burnham & Anderson, 2002). Model significance levels were calculated using effective sample size (and degrees of freedom) to account for serial autocorrelation after Bretherton et al. (1999).

3.2 | Flood turbidite deposits

For this study, we obtained sediment cores with undisturbed water-sediment interfaces in early May 2017 from the ice surface using an Uwitec hammer-driven gravity corer at 39 locations across Eklutna Lake (Figure 1(a)). Coring locations match those of previous studies (sites 1P-5P), initially established by Boes (2014), in addition to a longitudinal (long-axis) transect (sites 1–14) and five lateral (short-axis) transects (sites 15–34). Sediment cores ranged in length from 35 to 48 cm (42 cm mean). To minimize post-coring disturbance, we kept cores vertical and curtailed handling and transport until processing within a few days of collection at a nearby Alaska Pacific University (Anchorage) laboratory. Core tubes (9 cm diameter) were presplit lengthwise to enable a relatively rapid and more gentle splitting procedure.

After splitting, we lightly scraped the core surfaces parallel to lamina to reveal fine sedimentary structures. Core surfaces were photographed while wet, and again after air-drying to near maximum visual contrast. When wet, cores were volumetrically subsampled (1 cm^3) for dry bulk density (DBD; $g\ cm^{-3}$) using a 5 mL syringe at sediment depths 0–1 cm, 2.5–3.5 cm, 5–6 cm and onward down-core at a 5 cm interval. For DBD, samples were oven-dried overnight (85°C, 12 hours). Organic content was subsequently estimated from the DBD samples using loss on ignition (550°C, 5 h). Three different types of subsamples were collected using a microspatula for particle size analysis: (i) a bulk homogenized sample overlying the thick and widely distributed 1995 turbidite to the sediment surface for characterizing background sedimentation; (ii) full thickness homogenized samples of the two thickest recent turbidites (1995 and 1989); and (iii) 2.5-mm-thick samples obtained at 5 mm intervals through the 1995 and 1989

turbidites for sites 1P-5P to characterize within turbidite variability. Samples were pretreated with 30% H_2O_2 and heated overnight at 50°C to remove organics. Additionally, 10% Na_2CO_3 was added for 5 hours to remove biogenic silica. The pretreated samples were deflocculated using sodium metahexaphosphate and agitation before analysis on a Coulter LS230 laser diffraction analyser. Most samples were run in triplicate to assess instrumental result variability. Correlating and measuring the thicknesses and depths of turbidites previously identified for Eklutna Lake was carried out on the core surface imagery using vector drawing software (Inkscape).

We modified an empirical modelling approach after Evans and Church (2000) and Schiefer (2006) to quantify and contrast depositional patterns within Eklutna Lake for recent turbidites and background sedimentation. With this approach, regression surfaces based on bathymetric site attributes were fit to point measures of deposit thickness. As with the fluvial sediment transfer modelling, we used an exhaustive approach for model selection and used effective sample size for calculating significances. Continuous independent variables included distance from the primary inflow (*dist*; km) and water depth (*depth*; m), and factor variables included lake sub-basin (proximal basin = '*ProxB*'; distal basin = '*DistalB*') and lateral position (along longitudinal transect = '*Mid*'; left or southwest of longitudinal transect = '*SideL*'; right or north east of longitudinal transect = '*SideR*') (Figure 1(a)). Continuous independent variables were mean centered, with logarithmic and exponential transformations also evaluated to account for possible non-linear relations, and independent deposition variables were standardized. Pairwise interaction effects were also incorporated in the best model selections. Model coefficient results are interpretable in physical terms and may be used to describe systematic variability in depositional processes. Differences among model parameters between turbidites and background sedimentation can reflect changing sediment transfer dynamics over space and time.

3.3 | Sediment yield and regional flood correlation

To estimate longer-term (inter-decadal) sediment yield for the Eklutna Lake catchment with conservative error bounds, we used prediction intervals from the background sedimentation spatial modelling applied to a dense point grid (100-by-100 m; Figure 1(a)) over the lake bottom depositional area for fluvial suspended sediment accumulation. This depositional area was defined as the lake area excluding locations shallower than 10 m water depth, where fluvial suspended load sedimentation was assumed negligible due to high potential for littoral remobilization by water column mixing and slope effects, and excluding delta foreset slopes of the primary inflow, where sediment delivery is assumed to be bedload dominated. The 10 m threshold depth is from low (sampling) water level. Shallow-lateral deposition is shown to be minimal by the rapid thinning to absence of uppermost reflectors in sub-bottom profiles (Boes, 2014), and estimation of sediment yield was not sensitive to threshold depth selection because of lateral slope steepness. Specific sediment yield (Mg km^{-2} yr^{-1}) was calculated by multiplying background deposit thickness by dry sediment density and dividing by years of accumulation and contributing catchment area. We used the same spatial model-based methods to estimate the magnitude of turbidite sediment delivery. For regional flood correlation assessment, we use nearby USGS discharge records from the similarly sized, although less glacierized, catchments of Ship Creek (230 km^2; USGS 15276000), Little Susitna River (160 km^2; USGS 15290000), and Willow Creek (430 km^2; USGS 15294005) (Figure 1(e)) over analysis periods of up to 30 years (1987–2016).

4 | RESULTS

4.1 | Fluvial sediment transfer

Instrumentation failures and field access limitations restricted our usable fluvial SSC data to only 2015 (WF and EF), while usable and near-continuous turbidity data spanning 2.5 months or more of the open-channel season included 2009, 2011–2015 and 2017–2018 for WF, and 2009, 2012, 2015 and 2017 for EF. SSCs for WF were less right-skewed, greater in magnitude and range, and more correlated with creek discharge (log–log [power] relation) compared to EF (Figure 2). Multivariate modelling significantly reduced residual variability in $\log_e$SSCs, especially for EF (Table 1). Eight predictor variable terms were selected for each study creek by our optimized model fitting procedure, including three and two interaction terms involving $\log_e Q$ for WF and EF, respectively. Both creek models included $\log_e Q$, *Julian*, cos_{hr} and $temp_{24hr}$. The WF model also included *Qe* and the EF model additionally included sin_{hr} and $rain_{24hr}$. Other than for discharge, no predictor variable transformations significantly improved the models, hence logarithmic relations with SSC (i.e., untransformed-$\log_e$SSC relations). Relatively strong linear relations between SSC and turbidity (NTU) observed for both creeks in 2015 (Figure 3) suggests appropriateness of using the more continuous and temporally extensive turbidity data for further analyses of hydroclimatic controls on fluvial sediment transfer to Eklutna Lake.

Turbidity of the study creeks generally increases rapidly around early June and usually falls to some of the lowest observed values by late September (Figure 4). Early- to mid-summer turbidity tends to follow freshet discharge fluctuations with most peaks coinciding with high flows during warm temperatures and/or moderate rainfall. Most of the highest turbidity peaks occur during late summer and early autumn rainfall floods. Due to considerable variability in 2015 SSC-NTU relation and our inability to assess temporal consistency of that relation, in addition to instrumentation differences among years, we limit our interannual, NTU-based model assessments to consideration of full model statistics and coefficient signs to only assess the direction of select hydroclimatic controls. Furthermore, in preliminary model assessment work, we deemed interaction terms too spurious and inconsistent to include. Of the 12 NTU-based models (8 years WF; 4 years EF), significance of model fits was overall marginal and varied significantly, with seven model *p*-values exceeding 0.05 and an overall range of 0.003–0.255 (Table 2). EF models retained more

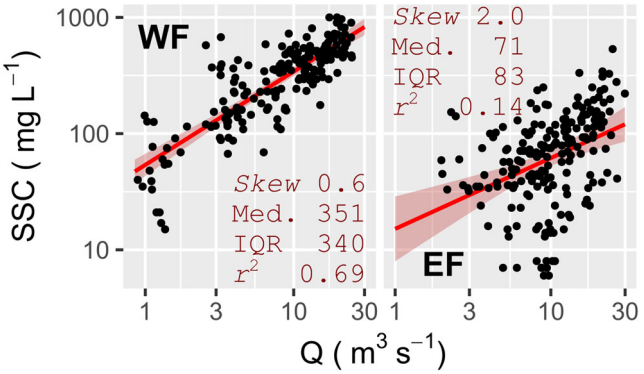


FIGURE 2 Suspended sediment concentration (SSC) by discharge (Q) log–log plots for West Fork (WF) and East Fork (EF) creeks in melt season 2015 with power relation regression lines and 95% confidence intervals. SSC statistics listed include skewness coefficient (*skew*), median (med.; mg L^{-1}), interquartile range (IQL; mg L^{-1}), and coefficient of determination (r^2) of logSSC-logQ regression fits

independent variable terms overall than the WF models. The only variable retained in every model for both creeks was discharge ($\log_e Q$), consistently with a positive effect on turbidity ($\log_e$NTU). We observed dominantly positive model term effects for *Qe*, *Julian* and sin_{hr} for both creeks. Fewer models retained ΔQ, which had positive coefficients for WF and negative for EF, and cos_{hr}, which had positive coefficients for EF (consistently negative cos_{hr} coefficients dropped for WF). For climate variables, EF had dominantly positive coefficients for both $temp_{24hr}$ and $rain_{24hr}$. Inclusion of climate variables in the WF models resulted in considerable overfitting and/or highly inconsistent fits, hence we dropped those variables in the final models; although, it was interesting to note the consistent negative $temp_{24hr}$ term in WF models.

4.2 | Flood turbidites

Sedimentary character of the 1989 and 1995 turbidites, attributed to regional rainstorm floods in August and September, respectively, have been described in detail by Boes et al. (2018) and Vandekerkhove et al. (2020). They display a dark to light coloured upward grading pattern similar to the varves but are thicker and with a coarser base. A thinner turbidite identified and described by Van Daele et al. (2020) was unambiguously dated to 2012 based on core-to-core correlations between 2012 and 2014 repeat coring and varve counts through that interval. This turbidite also correlates with a late September rainstorm flood in local and regional discharge records. Another thinner turbidite is marked in annotated core imagery and age-depth models of Boes et al. (2018) at about the midpoint depth between the 1995 turbidite and the 2012 sediment surface in cores retrieved from the Eklutna Lake proximal basin. This other minor turbidite was tentatively dated as 2004 or 2006, and possibly attributed to relatively high late summer to early autumn monthly precipitation in Anchorage (Boes, 2014). We attribute that turbidite to a 2006 August rainstorm flood based on the prominence of a corresponding discharge peak in three nearby streamflow records (Figure 5) and reported flood damage to property and infrastructure in the lower Susitna Basin (Lunsford & Rundquist, 2006). We use these four turbidites (major = 1989 and 1995, minor = 2006 and 2012) in our analyses of flood sediment

TABLE 1 Multivariate rating curve models of $\log_e$(SSC) for 2015 West Fork and East Fork creeks. Predictor variables are described in the text. Overall model values include sample size (n), residual standard error (SE), adjusted R^2, and effective degrees of freedom (DF_{eff}). Both full model *p*-values are <0.001. Model term values include predictor variable, coefficient, and standard error (SE). All model term *p*-values are <0.02, either individually or within an interaction

Creek-	West Fork (WF)	East Fork (EF)
n	196	202
resid. SE	0.383	0.551
adj. R^2	0.788	0.649
DF_{eff}	8, 16	8, 47
Intercept		
coeff.	2.352	−0.542
SE	0.597	0.672
Term 1		
Variable	$\log_e Q$	$\log_e Q$
coeff.	1.482	−0.253
SE	0.293	0.239
Term 2		
Variable	*Julian*	*Julian*
coeff.	0.017	0.019
SE	0.002	0.001
Term 3		
Variable	*Qe*	sin_{hr}
coeff.	0.002	−0.407
SE	0.0004	0.160
Term 4		
Variable	cos_{hr}	cos_{hr}
coeff.	−0.157	−0.664
SE	0.057	0.282
Term 5		
variable	$temp_{24hr}$	$temp_{24hr}$
coeff.	−0.129	−0.076
SE	0.039	0.054
Term 6		
variable	$\log_e Q$:*Julian*	$rain_{24hr}$
coeff.	−0.008	−0.184
SE	0.001	0.068
Term 7		
variable	$\log_e Q$:*Qe*	$\log_e Q$:$rain_{24hr}$
coeff.	−0.001	0.065
SE	0.0002	0.024
Term 8		
variable	$\log_e Q$:$temp_{24hr}$	$\log_e Q$:$temp_{24hr}$
coeff.	0.059	0.088
SE	0.017	0.021

delivery and deposition in Eklutna Lake (Figure 6). Although less in spatial extent and mean thicknesses, the thinner turbidites of 2006 (measurable at 68% of coring sites; 0.78 cm mean thickness) and 2012 (68%, 1.14 cm), are visibly similar to the thicker and more studied turbidites of 1989 (95%, 1.49 cm) and 1995 (97%, 2.88 cm).

We observe some consistent spatial patterns among the studied flood turbidites in Eklutna Lake. In addition to the overall thinning trend downlake, the turbidites locally thicken around 2, 5 and 8 km from the primary inflow (Figure 6(b)). Turbidites at lateral transect sites are slightly thinner on average, and in many locations are similar or slightly thicker, relative to corresponding thicknesses along the central longitudinal profile. Except for the distal basin core 1P lateral transect, turbidite thicknesses tended to be thicker in left-side cores for the thickest 1995 turbidite, with less clear lateral trends for the other turbidites. Background sedimentation rates also decrease downlake, but with deviations to slightly higher rates around 3.5 and 7.5 km from the inflow, and consistently higher rates in right-side cores, especially in the proximal basin (Figure 6(c)). Relative to background sedimentation, turbidite thicknesses are greatest in the distal end of the proximal lake basin, at about 4.5–5 km downlake for the 2012, 2006 and 1989 turbidites, and further downlake at about 6 km from the inflow for the overall thickest 1995 turbidite (Figure 6(d)). Secondary peaks of high turbidite thickness relative to background occur near the proximal end of the lake at 2–2.5 km downlake, and near the distal end of the lake at 8–8.5 km downlake from the primary inflow. Greater left-side deposition is especially pronounced in relative thickness of the 1995 turbidite in the proximal basin. Median particle size (d_{50}) decreases near-linearly downlake for the homogenized samples representing background sedimentation (Figure 6(e)). Homogenized samples of the 1995 turbidite average about 2.5 μm coarser than background; whereas homogenized 1989 samples were only slightly coarser than background. The 1995 turbidite is particularly coarse closest to the inflow and on the sill separating the proximal and distal lake basins. We note considerable d_{50} variability in the triplicate analyses of the 1995 turbidite bulk samples (median triplicate sample range is 1.1 μm; three ranges exceed 10 μm). Lateral transect cores tend to be finer than corresponding central samples, although only the thickest 1995 turbidite could be extensively sampled for particle size. Intra-turbidite particle size analyses show systematic upward fining and upward left to right distribution skewing in log-transform space (Figures 6(a) and 7).

Our spatial modelling of deposit thicknesses quantifies some patterns of Eklutna Lake sedimentation. Because of the widespread prominence and distinctiveness of the 1995 turbidite, we estimate background sedimentation rates using the sediment surface to the 1995 cap sediment thicknesses. This interval, which includes the relatively thin 2006 and 2012 turbidites, allows us to incorporate all but one coring site (site 28, Figure 1), covering a thicknesses range of 22.1–3.4 cm from the most inflow proximal (core 13) to distal (core 01) sites, respectively, and yields a similar background rate in the distal basin from Pb/Cs radiometric dating by Praet et al. (2017). When modelling only those sites along the longitudinal transect, the sediment interval representing background sedimentation thins at about 1.1 cm (0.3 standardized units) per km from the primary inflow and thickens at about 0.1 cm (0.025 units) per meter of water depth (Figure 8). Distance and depth coefficients do not significantly differ between the background longitudinal pattern and 2006 and 2012 minor turbidites. Relative to background and minor turbidites, the 1989 and 1995 major turbidites thin less with distance from the inflow, at about 0.1 standardized units per km, and are thicker with increasing water depth, at about 0.05 units per meter of water depth. Spatial modelling with the full core dataset, using factor variables for discriminating lake basin (*ProxB* or *DistalB*) and lateral transect position (*SideL*, *SideR* or *Mid*), and the factor-to-continuous variable (*dist* and *depth*) interactions, was conducted for background sedimentation and the two major turbidites. The two minor turbidites were excluded from this analysis because they were not distinguishable in many of the shallower lateral and distal basin sites (Figure 6). These expanded models capture additional spatial nuances, including significant basin side interaction effects in background sedimentation, side and basin interactions with the thickest 1995 turbidite, and a basin interaction effect with the 1989 turbidite (Table 3).

4.3 | Sediment yield and regional flood correlation

We estimate recent lake-based background specific sediment yield to be 109 ± 44 Mg km^{-2} yr^{-1} (95% confidence; 1996–2017), obtained from the product of our modelled, spatially-integrated, background deposition rate and measured sediment density. Dry bulk density of Eklutna Lake sediment averages 0.79 g cm^{-3}, with an organic-matter content of 4.3%. This magnitude of sediment delivery is consistent with our fluvial monitoring data, with approximate yields on the order of 100–200 Mg km^{-2} yr^{-1} over the period of record, if the 2015 Q-SSC rating is representative (95% confidence interval). The 1995 turbidite is denser (0.90 g cm^{-3}) and slightly less organic (3.9%) than the background sediment. Physical characteristics of the 1989 turbidite, where measured, are similar to those measured for the 1995 turbidite. The 2006 and 2012 turbidites were too thin for volumetric sampling. Applying 0.90 g cm^{-3} for turbidite density to the spatially distributed estimates of turbidite thickness from our spatial models, the factor that turbidite sediment yields exceed longer-term annual delivery, in decreasing rank order, are 15 (1995), seven (1989), five (2012) and three (2006) times greater than background sediment yield.

The 2012 turbidite, attributed to a late September rainstorm, is the only flood turbidite of study that was deposited during fluvial monitoring of Eklutna Lake inflow (Figure 4). The 20 highest hourly discharges of record for WF and EF occur that year on 22-September and 23-September, with maxima of 71 and 100 m^3 s^{-1} for WF and EF, respectively. Data gaps exist those days for EF, but the WF series is complete through the flood, which was preceded by heavy precipitation in the Eklutna catchment. In regional discharge record comparisons over a 30-year period of 1987–2016, in order of decreasing sediment delivery, the four flood turbidite years 1995, 1989, 2012 and 2006 correlate with Ship Creek annual peak daily discharges of rank 3, 4, 1 and 12, respectively (Figure 9). For annual peak discharges during the late summer-early autumn months of August and September, the four study turbidites coincide with the top four peak annual daily discharges, but still not in

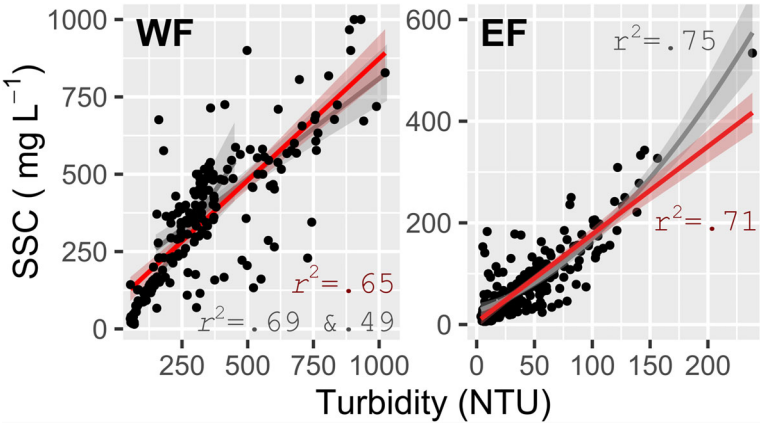


FIGURE 3 Suspended sediment concentration (SSC) by turbidity (NTU) plots for West Fork (WF) and East Fork (EF) creeks with linear regression lines (red) and 95% confidence intervals (light red). Slightly better fits were obtained by NTU < 400 piecewise fitting and quadratic fitting for WF and EF creeks (grey), respectively

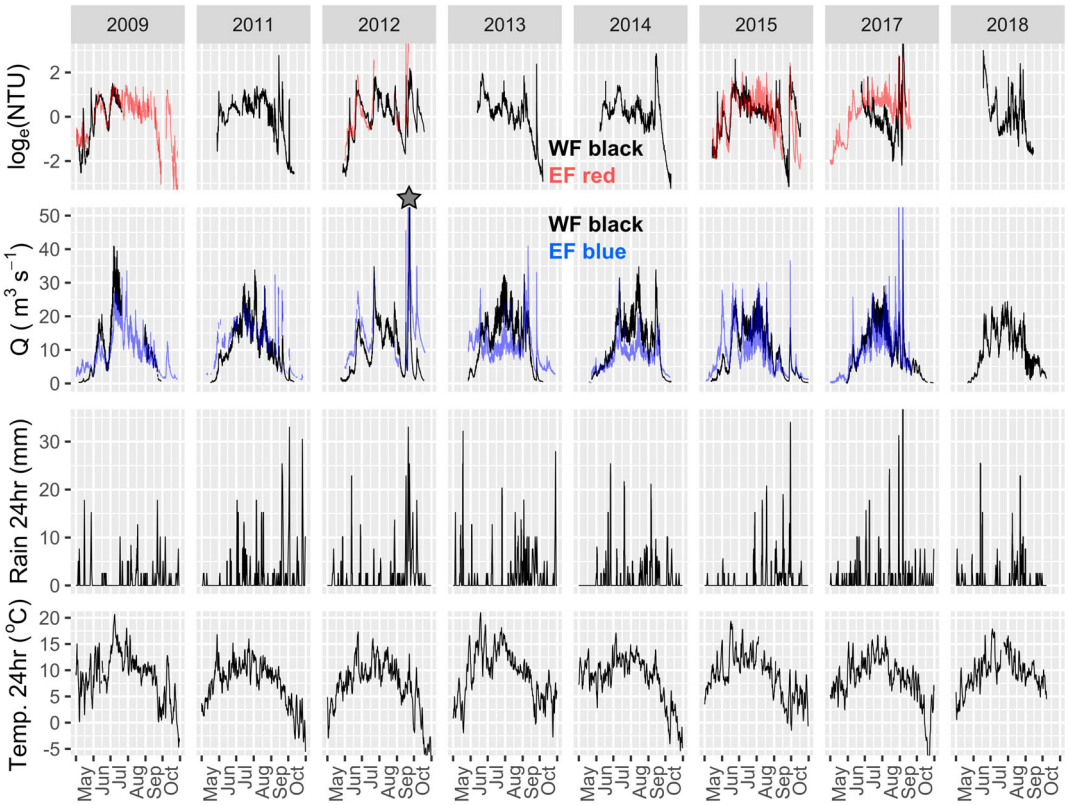


FIGURE 4 Primary fluvial and meteorological time series data used for sediment rating curve modelling, including hourly turbidity (NTU) and discharge (Q) for West Fork (WF) and East Fork (EF) creeks, and daily rainfall and temperature from the SNOTEL site (Figure 1(b)). Peak WF Q of record (star) was 71 m^3 s^{-1} on 23-September-2012 (gap in EF Q data at this day-time)

matching rank order. For the Little Susitna River discharge record over the same period, the two highest peak annual daily discharges correlate with the two minor 2006 and 2012 turbidites, but no significantly high flows were observed for the 1989 and 1995 major turbidite years.

5 | DISCUSSION

5.1 | Fluvial sediment transfer

Elevated SSCs on average, and greater specific yield overall, for the more glacierized WF catchment relative to EF is consistent with increased loads from more glacierized catchments, which has been generally observed globally and for southern Alaska (Hallet et al., 1996). Multivariate models relating hydrometric controls to SSCs show the importance of discharge, but with varying effects implied by variable interactions (Table 1). For WF, within predictor ranges, the log$_e$*Q*:*Julian* term indicates a decreasing positive discharge effect on SSC through the open-channel season, approaching a negligible discharge influence if all other predictors are constant. This can reflect high loading of glaciogenic sediment over a wider discharge range when subglacial conduits are more extensive and coupled with catchment drainage (Delaney et al., 2018; Kido et al., 2007). The other interactions of log$_e$*Q*:*Qe* and log$_e$*Q*:*temp*$_{24hr}$ indicate that positive

TABLE 2 Multivariate models of West Fork and East Fork standardized turbidity (log_eNTU) by year. Predictor variables are described in the text. Overall model parameters include sample size (n), residual standard error (SE), adjusted R^2, effective degrees of freedom (DF_{eff}), and *p*-value. Only the sign of variable coefficients is shown (in bold if individual term *p*-value <0.05). Variables dropped in the backward stepwise regression process described in the text are in grey

Creek -	West Fork (WF)								East Fork (EF)			
Year -	2009[a]	2011	2012	2013	2014	2015	2017[b]	2018[b]	2009	2012[c]	2015	2017
n	1736	3112	3449	2783	3017	3725	1910	2104	2951	1494	3291	3578
resid. SE	0.415	0.424	0.560	0.420	0.571	0.592	0.919	0.865	0.401	0.355	0.463	0.272
adj. R^2	0.828	0.820	0.687	0.824	0.674	0.650	0.156	0.252	0.845	0.874	0.786	0.926
DF_{eff}	1.056	4.790	3.164	3.164	2.609	11.81	93.86	12.97	9.684	3.088	8.779	3.529
p-value	0.255	0.049	0.074	0.064	0.116	0.017	0.003	0.057	0.003	0.067	0.020	0.060
log_eQ	**+**	**+**	**+**	**+**	**+**	**+**	**+**	**+**	**+**	**+**	**+**	**+**
ΔQ_{1hr}		+				**+**			–			–
Qe	–	**+**	+	+	+	**+**	**+**	+	**+**	*na*	–	+
Julian	–	–	+	–	–	**+**	**+**	–	**+**	**+**	**+**	**+**
cos_{hr}	–		–	–	–			–		+	**+**	**+**
sin_{hr}		**+**		+	+	**+**	**+**	+	–		**+**	**+**
$temp_{24hr}$	–	–	–	–	–	–	–	–	**+**	+	**+**	**+**
$rain_{24hr}$	+		–	+	–	–	+	+	–	**+**	**+**	+

[a]only early season data (to 7/20).
[b]missing over 6 weeks of early and/or late season data.
[c]large mid-season data gap (7/22 to 8/28).

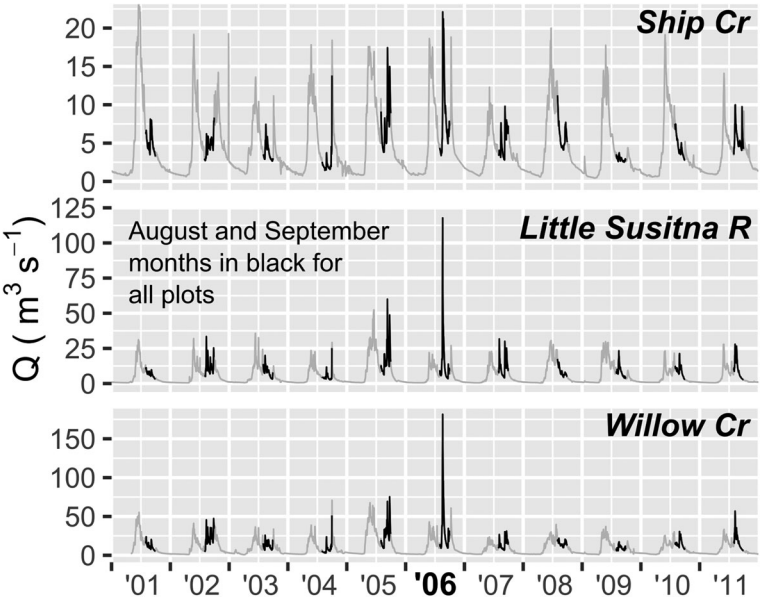


FIGURE 5 Comparison of daily discharges from three regional streams (Figure 1(e)) for the period 2006 ± 5 years. The ±5 year interval greatly exceeds corresponding varve counting uncertainty by Boes et al. (2018). For the comparison interval, 2006 was the largest annual flood year in two of the three records (little Susitna River and Willow Creek), and the second largest in the other (Ship Creek). 2006 was the largest annual flood in all three records for the late summer to early autumn months of august–September when greatest flood sediment delivery is expected for the Eklutna Lake catchment

discharge effects on SSC increase at higher temperatures and, even more significantly, when discharges have not been exceeded for longer durations. To some degree, those two interaction effects negate the log_eQ:*Julian* seasonal trend during warm conditions when discharge exceeds flows of prior weeks. Positive SSC relations with longer event spacing and at higher temperatures have been observed in other proglacial settings, reflecting increased supply from recharged sediment storages (e.g., Hodgkins, 1999; Schiefer et al., 2017) and glacial sediment released through accelerated melt (e.g., Loso, 2009; Menounos et al., 2005), respectively. Although various *Q* to SSC relations are often applied in standard sediment rating curve approaches, we are unaware of other studies where interactions were used to explore such multifaceted aspects of sediment transfer. The remaining WF model term of cos_{hr} indicates diurnal SSC peaks near 12:00, which coincides with the rising hydrograph limb, and is indicative of clockwise hysteresis common to some proglacial catchments (e.g., Richards & Moore, 2003; Singh et al., 2005). For EF, the log_eQ:$temp_{24hr}$ interaction indicates greater discharge effects on SSC at

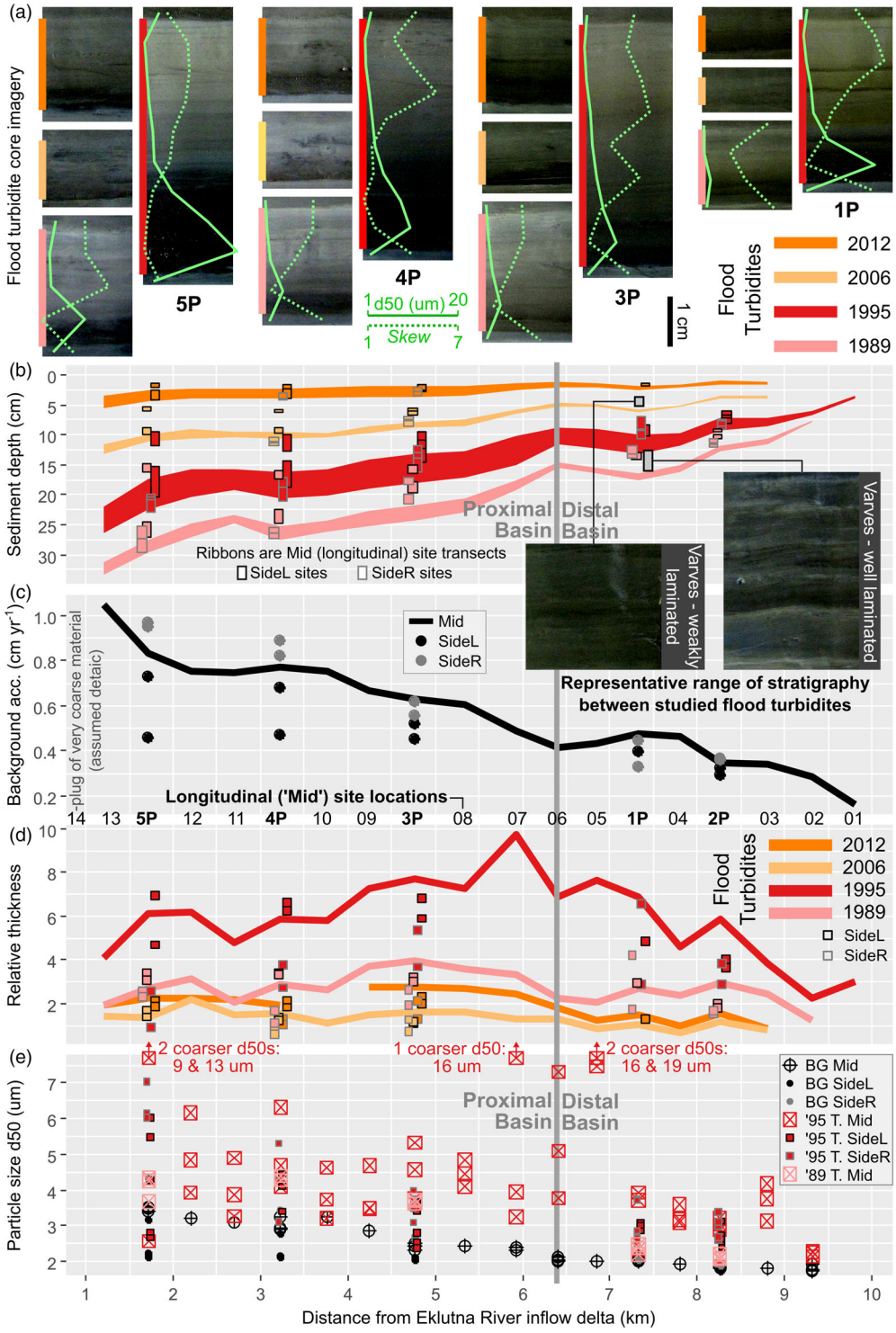


FIGURE 6 Stratigraphy and measured physical characteristics of recent major (1995 and 1989) and minor (2012 and 2006) flood turbidites and/or background sedimentation in Eklutna Lake (Figure 1(a)), including: (a). Master core imagery of turbidites (consistent scale, 15% linear contrast stretch) with particle size d50 and skewness; (b) Turbidite sediment depths and thicknesses; (c) background sedimentation rates; (d) Turbidite thicknesses relative to background sedimentation; (e) bulk particle size d50 data

higher temperatures, like that of WF, and $\log_e Q{:}rain_{24hr}$ suggests negligible to slightly negative effect of light rainfall on SSCs that dramatically shifts towards large SSC increases for moderate to high rainfall. A negative rainfall-SSC relation for light precipitation could result from dilution (e.g., Schiefer et al., 2017); whereas, the positive relation for heavier precipitation likely reflects associations of increased sediment transfer by rain-on-glacier induced flushing of glacial conduits, as well as raindrop and overland flow processes (e.g., Leggat et al., 2015 ; Richards & Moore, 2003). The non-interacting EF terms indicate increasing SSCs through the open-channel season which could relate to increased glacial/proglacial entrainment, and mid-afternoon diurnal SSC peaks which, like for WF, coincides with rising hydrograph limbs.

While limited to only one year of SSC-based modelling (2015), our inter-annual NTU data allowed us to further assess hydroclimatic controls on sediment transfer. Overall significances of our NTU-based

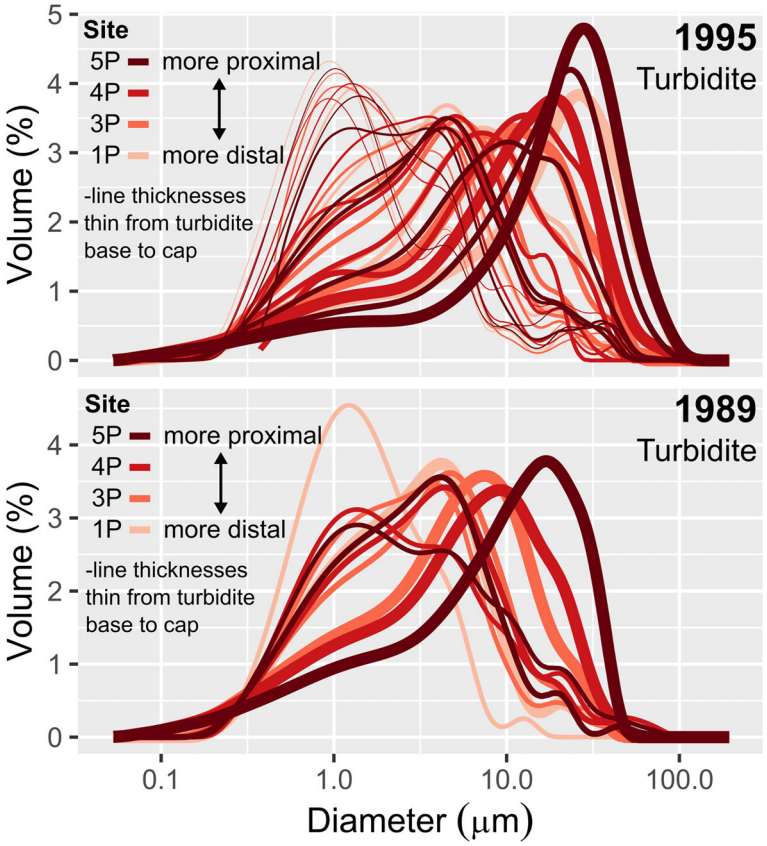


FIGURE 7 Particle size distributions within major turbidites (1995 and 1989) from 2.5-mm-thick sub-samples obtained at 5 mm intervals for master core sites (5P-1P; Figure 1(a))

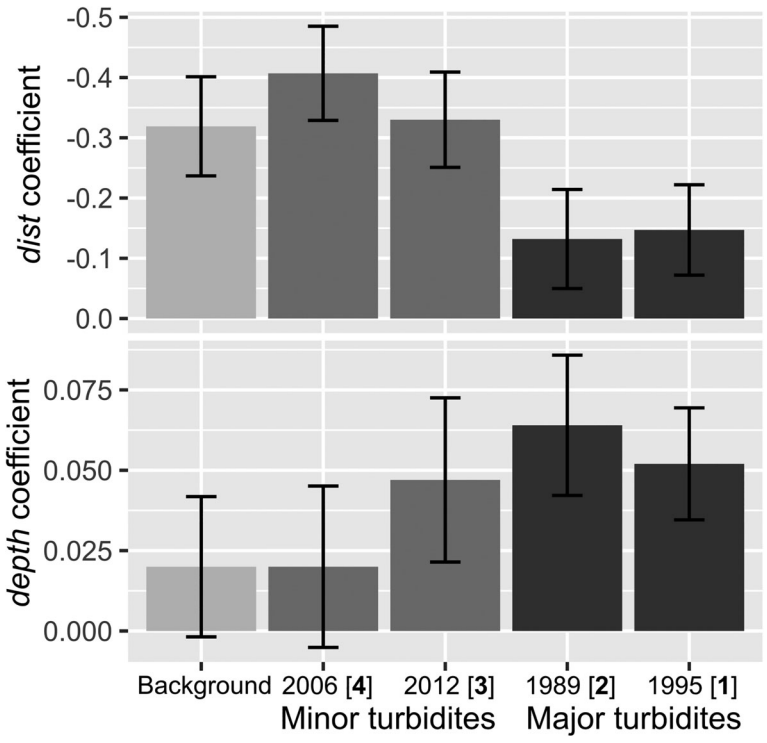


FIGURE 8 Coefficients from spatial modelling of within-lake deposition patterns incorporating only site distance from the primary inflow (*dist*; km) and water depth (*depth*; m) predictor variables for background sedimentation (about 1996–2016) and the four study turbidites (in reverse magnitude rank order). Coefficients are for standardized rates of deposition, as described in text

models were one to three orders weaker than our SSC-based modelling, and because of NTU data limitations, interaction terms were not explored. A positive relation between discharge ($\log_e$Q) and turbidity ($\log_e$NTU) is the most significant and consistent effect across NTU-based models (Table 2), reflecting the dominant control of discharge on suspended loads. Fewest additional coefficients were retained for the recorded peak discharge year (2012; Figure 4) suggesting that discharge control may be especially dominant during flood years. The

TABLE 3 Expanded modelling of with-lake spatial patterns of sedimentation. All variables are described in text, including standardized dependent variables of deposition, continuous (mean-centered) independent variables *dist* (km) and *depth* (m), and independent factors with *mid* (central position) and *ProxB* (proximal basin) as reference locations. Model term values include predictor variable, coefficient, standard error (SE) and significance[a]. Overall model values include residual standard error (SE), adjusted R^2, effective F statistic (F-stat$_{eff}$, including degrees of freedom, DF), and significance[a]

	Background deposition			Turbidite T1 (1995)			Turbidite T2 (1989)		
Term	**Coeff.**	**SE**	**Sig.**	**Coeff.**	**SE**	**Sig.**	**Coeff.**	**SE**	**Sig.**
dist	−0.32	0.04	***	0.07	0.06		0.05	0.06	
depth	0.01	0.01		0.05	0.01	***	0.10	0.01	***
SideL	−0.49	0.12	***	−0.41	0.15	*			
SideR	0.07	0.14		−0.64	0.18	**			
SideL:dist	0.26	0.07	***						
SideR:dist	−0.16	0.08	.						
SideL:depth	0.05	0.02	*	0.02	0.02				
SideR:depth	−0.03	0.02		−0.01	0.02				
DistalB				−0.25	0.33		−0.77	0.25	**
DistalB:dist				−0.32	0.14	*			
DistalB:depth							0.05	0.02	*
	SE = 0.27, adj R^2 = 0.91 F-stat$_{eff}$ 24.9 (8,14.3 DF) ***			SE = 0.34, adj R^2 = 0.88 F-stat$_{eff}$ 9.1 (8,7.0 DF) **			SE = 0.34, adj R^2 = 0.88 F-stat$_{eff}$ 59.5 (4,13.4 DF) ***		

[a]*p*-value levels: '***' ($p < 0.001$), '**' ($p = 0.001$ to 0.01), '*' ($p = 0.01$ to 0.05), and '.' ($p = 0.05$ to 0.1).

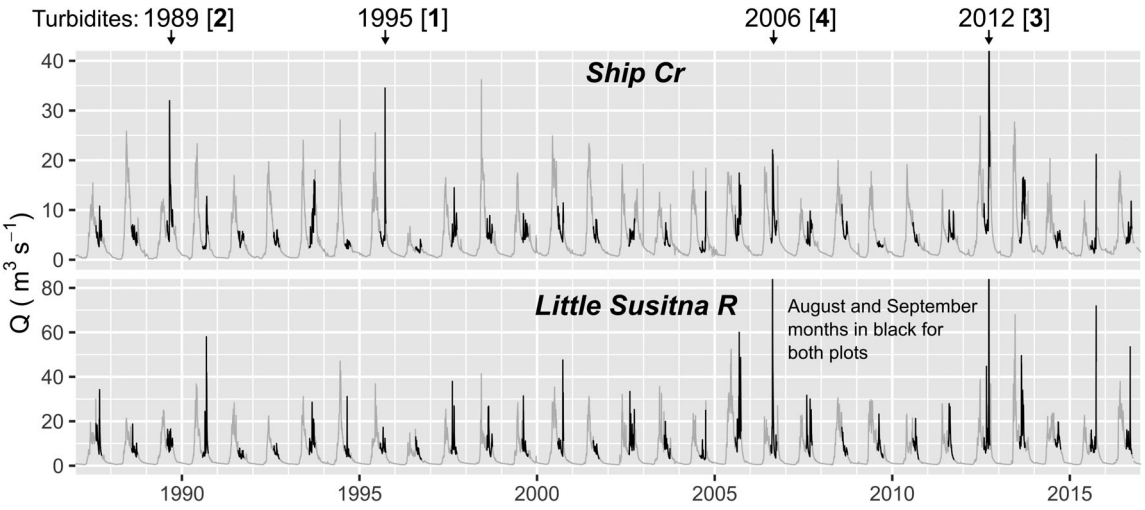


FIGURE 9 Regional discharge records over 30-year period (1987–2016) with correlated flood turbidites of this study (turbidite magnitude ranks in square brackets). Willow Cr (Figures 1(e), 5) excluded from this longer-term regional assessment because of missing data (<2001)

seasonal trend (*Julian*) and discharge exceedance (*Qe*) terms both tended to be positive effects for the study creeks, which is consistent with the SSC-based models for WF (both terms) and EF (*Julian*), potentially reflecting seasonal source expansion and effects of event spacing. ΔQ_{1hr} was only retained in a pair of models for each creek, but with a positive sign for WF and negative for EF. This was not a retained variable in SSC models, and may reflect hysteresis effects not captured in the trigonometric terms, with more distant glacial/proglacial sediment sources of EF potentially explaining the ΔQ_{1hr} sign reversal (Williams, 1989). The WF negative tending cos_{hr} term is consistent with the SSC model, but additional retention of sin_{hr} suggests an earlier NTU diurnal peak in the late morning instead of around noon. This shift earlier could reflect NTU measurement not evenly capturing variability in suspended sediment, for example, missing a coarser fraction at greater diurnal flows, but opposing EF signs (positive cos_{hr} and sin_{hr}) compared to the SSC model is difficult to explain. The climate variable terms for EF are typical for interpreting meteorological influences on sediment transfer, with positive $temp_{24hr}$ coefficients and mostly positive $rain_{24hr}$ coefficients suggesting influences of accelerated glacier melt (Loso, 2009; Menounos et al., 2005) and rain-enhanced erosion (Leggat et al., 2015; Richards & Moore, 2003). The WF climate terms were not retained in final models, with

inconsistent $rain_{24hr}$ coefficient signs and the unusual result of consistently negative $temp_{24hr}$ signs (Hodder et al., 2007) which also contrast the SSC model. Some of the overall differences between WF and EF models could be explained by more readily available channel and near-channel sediment in the WF catchment, resulting in simpler discharge-dominated relations and fewer retained predictors; whereas less available and more distant sediment sources in EF result in model improvement with more predictors reflecting delayed delivery and hydroclimatic controls. We cannot dismiss data limitations playing a role in the inconsistencies between SSC- and NTU-based models. Other than the EF trigonometric terms, there is good consistency among retained variable effects in the overlapping year (2015). For both creeks the dominant control on suspended loads (SSC and NTU) is discharge, with the SSC-based models suggesting more multifaceted interactions, and the NTU-based models indicating interannual consistency of discharge controls.

5.2 | Flood turbidites

Turbidites rapidly deposited by exceptional sediment loads delivered by floods are stratigraphically distinct from lower-energy background deposition in the Eklutna sediment record (Figure 6, and as previously described in detail by Boes et al. (2018). Some spatial pattern differences are associated with varying physical processes of sediment transfer across the lake subbasins. Simple spatial modelling of sedimentation along the longitudinal profile captures proximal to distal (downlake) thinning in the negative *dist* coefficients and sediment focusing to deeper water settings in the positive *depth* coefficients (Figure 8). Minor turbidite (2006, 2012) thinning and focusing did not differ from the background sedimentation spatial pattern; however, the major turbidites (1989, 1995) show significantly reduced rates of downlake thinning and considerably greater deep-water sediment focusing. The reduced rate of thinning relative to background and minor turbidite deposition may reflect stronger inflow currents effectively transferring sediment to more distal settings, similar to the spatial signature of flood deposits described in proglacial Green Lake, British Columbia (Schiefer, 2006). Dominance of underflows and/or deeper interflows from highly turbid fluvial sediment delivery during major floods likely explains elevated sediment focusing with the major turbidites, a depositional pattern that has been well documented for flood deposits in a wide range of settings, and especially for proglacial lakes (Schillereff et al., 2014; Smith & Ashley, 1985). The magnitude of focusing for the studied flood turbidites is not as great as that for documented earthquake-generated turbidites (Praet et al., 2017), but elevated focusing from exceptional floods could sufficiently overtake lake stratification and other mixing controls to confound discrimination between turbidite trigger mechanisms if other sedimentological characteristics are not carefully considered (e.g., Vandekerkhove et al., 2020).

Our expanded spatial modelling, which incorporates interacting categorical variables of lake basin (*ProxB-DistalB*) and lateral position (*SideL-Mid-SideR*), further differentiates background deposition and the two major flood turbidites (Table 3). The negative *dist* and positive *depth* coefficients for background again reflect the expected downlake decline in accumulation and sediment focusing into deep water settings, respectively, along the longitudinal profile (Figure 8). The *SideL* and *SideR* coefficients show reduced deposition along the left (southwest) lake margin and marginally greater deposition along the right (northeast) margin relative to longitudinal profile cores (Figure 6 (c)). Furthermore, the *SideL:DistalB* and *SideL:depth* interactions indicate a less negative (reduced) distance effect and a more positive (increased) depth focusing effect, respectively, along the left lake side. Since the left margin is the primary inflow side of the lake (Figure 1), these background model terms are consistent with sediment bypassing left-proximal settings and increased dispersion to right-distal settings. This pattern may reflect sediment transfer, particularly for the finer fluvial sediment fraction, by inflow currents with potential rightward deflection effects driven by lake basin curvature (Hamblin & Carmack, 1978), Coriolis effect (Smith, 1978; Wells, 2009) and/or wind mixing (Desloges & Gilbert, 1991; Gilbert & Shaw, 1981). Increased left-side depth focusing is a more minor effect, but it could capture left-proximal (near-delta) deposition of coarser sediment. For the thickest 1995 flood turbidite, the oppositely signed (positive) *dist* coefficient indicates a lack of proximal basin thinning downlake, which could reflect the strong inflow current push, especially for the finer fluvial fraction (Schiefer, 2006). The larger *depth* coefficient relative to background, reduced left (*SideL*) and right (*SideR*) lake margin deposition, and more positive left-proximal (*SideL:depth*) deposition are all consistent with significantly increased near-delta and thalweg sediment focusing by strong turbidity current underflows (e.g., Desloges & Gilbert, 1991; Lamoureux et al., 2002; Schiefer, 2006). The 1995 turbidite negative *DistalB* and *DistalB:dist* terms reflect the expectedly lower distal basin deposition, which may be more pronounced by extreme sediment trapping in the proximal basin by flood-driven turbidity currents, and a more typical downlake thinning pattern in the distal basin, respectively. The major 1989 flood turbidite model shows the same lack of proximal downlake thinning and enhanced depth focusing, although without any lake side differentiation. The 1989 *DistalB* term captures reduced distal basin deposition like in the 1995 turbidite model, but in this case the *DistalB* interaction suggests reduced distal basin focusing. These last terms in the 1989 model, especially much lower *DistalB* term relative to 1995, may indicate relatively greater side tributary sediment input mid-way downlake during the 1995 flood, which may also reflect the position of peak 1995 turbidite relative thickness and most anomalously coarse particles (Figure 6(e), also Praet et al., 2020) near the large Yuditnu Creek tributary fan-delta (Figure 1(a)).

5.3 | Sediment yield and regional flood correlation

Our interdecadal, lake sediment-based estimate of 109 ± 44 Mg km^{-2} yr^{-1} for specific yield to Eklutna Lake is within regional yield patterns reported for partially glacierized catchments in Alaska (Hallet et al., 1996) and glacierized lake catchments in the Canadian

Cordillera (Schiefer et al., 2001). The relatively instantaneous, flood-based sediment delivery recorded in the four recent turbidites of study correspond to relative yields 3–15 times greater than annual background delivery. Relating the turbidites to hydroclimatic data from within the catchment was limited as temporal overlap only exists for the 2012 minor turbidite. Highest discharges of record (2009–2018 WF, 2009–2017 EF) occurred that year in late September following heavy local precipitation (Figure 4). A regional assessment of turbidite-flood correlation was possible using discharge data for the Ship Creek catchment 30 km to the southwest and also situated in the western Chugach Mountains, and the Little Susitna catchment 55 km to the north in the Talkeetna Mountains (Figure 1(e)), both of which have continuous temporal data coverage spanning the years of our turbidite deposition study (Figure 9). With all four dated turbidites coinciding with the four greatest late summer to early autumn peak annual discharges of Ship Creek over our 30-year calibration period, Eklutna Lake turbidites show good potential as a seasonal flood proxy for the western Chugach Mountains. We note disorder, however, between turbidite volume and peak discharge rank magnitudes, suggesting reconstruction between turbidites and regional floods may be limited to a threshold flood exceedance as opposed to more a continuous magnitude-frequency relation. The minor 2006 turbidite, correlating with a Ship Creek peak discharge of 22 $m^3\ s^{-1}$, may be near or below such a flood threshold, as that only marginally exceeds a 2015 September peak of 21 $m^3\ s^{-1}$. Antecedent conditions were considerably different between those 2 years as 2006 exhibited a wet, high mean discharge summer whereas 2015 was among the driest recorded. The Little Susitna River discharge record shows significant flood peaks coinciding with the two minor turbidite years of 2006 and 2012, but no high flows coinciding with the major 1989 and 1995 turbidites, suggesting that such a flood proxy may be spatially limited to a large degree to the western Chugach Mountains. This regional variability is consistent with hydrological synoptic summaries, with most reported flood damage and abnormally heavy precipitation geographically focused in the Susitna Basin during the 2006 and 2012 events (Alaska Climate Research Center, 2012; Lunsford & Rundquist, 2006), as opposed to the western Chugach Mountains near Anchorage during the 1989 and 1995 events (Lamke et al., 1990; NOAA, 1996).

Longer-term assessment of the flood turbidite record could be beneficial since flood discharges from the western Chugach Mountains directly impact Anchorage, Alaska's most populous city, and the major Knik Arm transportation and utility (electric, water and gas) corridor (Figure 1(e)). Further flood proxy research would be aided by the 2300-year varve chronology and detailed flood versus earthquake turbidite discrimination studies conducted at Eklutna Lake (Fortin et al., 2019; Praet et al., 2020; Vandekerkhove et al., 2020). Issues complicating long-term flood proxy applications include limited use of recent instrumental data for calibration as sedimentation patterns were modified by outflow controls following conversion of the lake to a hydropower reservoir in 1928 (Boes et al., 2018), as well as documented occurrences of erosive earthquake-triggered turbidites and slumps causing inter-site unconformities and core chronology differences in the longer sedimentary sequence (Fortin et al., 2019; Praet et al., 2017). The extent to which turbidites may evolve from flood-triggered deltaic slumps and other remobilized lake sediment relative to the river transported load is unknown. Additionally, there are the generally known biases associated with such flood proxy applications, including hydroclimatic non-stationarity, such as that documented in lake sediment records of this region with the Little Ice Age transition (Boes et al., 2018), as well as localized, non-flood geomorphic disturbances, which can be especially significant in high-relief, proglacial settings (Mao et al., 2019).

6 | CONCLUSION

Fluvial data from the Eklutna Lake catchment show a dominating influence of discharge on sediment transfer, with multiple interconnections among related hydroclimatic controls. The complex and varying character of many of these connections may highlight limitations of using such statistical approaches. An improved understanding of sediment transfer dynamics could come from physically-based system assessments (Hodder et al., 2007). Aiding steps in that direction, ongoing efforts for the watershed system include distributed hydrologic simulation (Ostman, in progress), glaciological studies (Geck et al., 2021), and publication of our original, high-quality datasets (Ostman et al., in progress). Eklutna Lake is situated near major population and economic centers of south-central Alaska, including the city of Anchorage and lower Matanuska-Susitna basin. Ongoing and future studies here will further improve our ability to interpret catchment dynamics driving sediment transfer, including for exceptional floods in this region that is experiencing rapid environmental change.

Our extensive spatial network of short lake sediment cores captured the broad extent and range in character of distinctive flood turbidites, which we correlate to specific hydrological events in regional discharge records. Within-lake spatial modelling of turbidites quantifies variable rates of downlake thinning and sediment focusing effects. We describe especially large differences among the two thickest flood turbidites of study and background patterns of deposition, which we relate to strongly contrasting physical dispersion processes controlled by varying inflow current strength and turbidity, in addition to other relatively minor longitudinal and lateral lake circulation effects. Vastly greater depth focusing and downlake sediment transport within the proximal lake basin was captured in the major flood turbidite spatial signatures.

Interdecadal sediment yield to Eklutna Lake is typical for this glacierized region. Over the study period, the four largest flood turbidites show a magnitude of relatively instantaneous deposition 3–15 times greater than annual background accumulation. These turbidites correspond with late-summer and early-autumn rainstorms associated with broad cyclonic-frontal systems from the seasonally well-established Aleutian Low. These storms cause significant flood damage across this economically critical region of south-central Alaska. Synoptic storm variability may limit the regional applicability of flood proxy reconstruction across this broader inhabited zone to a certain threshold magnitude and forcing condition. Local

applications of the Eklutna Lake flood turbidite record are also considerable due to key infrastructure situated in the watershed, in the surrounding Chugach Mountains, and along the adjacent Knik Arm coast, with such work being strongly bolstered by the exceptional site records of associated physical processes and paleoenvironmental studies.

ACKNOWLEDGEMENTS

This research was funded through the NSF-Office of Polar Programs, Arctic System Science award ARC-1418000 and the NASA-Higher Education Alaska Space Grant Program. Hydrological monitoring support was provided by the Municipality of Anchorage utilities: Municipal Light & Power, and Anchorage Water & Wastewater Utility. We thank two anonymous reviewers for comments and suggestions which improved the content of this article.

DATA AVAILABILITY STATEMENT

Fluvial monitoring data that support the findings of this study are available from Ostman et al. (in progress) and from the corresponding author upon request. Lake sediment and limnology data are available from the corresponding author upon request. Regional daily discharge data used in in this study are publicly available from USGS Water Resources, National Water Information System (https://waterdata.usgs.gov/nwis).

ORCID

Erik Schiefer https://orcid.org/0000-0002-3546-2980
Jason Geck https://orcid.org/0000-0002-8479-1588
Johnse S. Ostman https://orcid.org/0000-0001-8060-7635
Nicholas P. McKay https://orcid.org/0000-0003-3598-5113
Nore Praet https://orcid.org/0000-0002-5567-3718
Michael G. Loso https://orcid.org/0000-0001-8414-2310
Darrell S. Kaufman https://orcid.org/0000-0002-7572-1414

REFERENCES

Alaska Climate Research Center. (2012). *September 2012 synoptic summary*. The Alaska Climate Research Center. http://climate.gi.alaska.edu/Summary/Synoptic/2012/Sep

Amann, B., Szidat, S., & Grosjean, M. (2015). A millennial-long record of warm season precipitation and flood frequency for the North-Western Alps inferred from varved lake sediments: Implications for the future. *Quaternary Science Reviews*, *115*, 89–100. https://doi.org/10.1016/j.quascirev.2015.03.002

Boes, E. (2014). Reconstruction of the southern Alaskan climate during the last 700 years, based on a multi-proxy analysis of annually laminated lake records. MS Thesis. University of Gent, Belgium.

Boes, E., Van Daele, M., Moernaut, J., Schmidt, S., Jensen, B. J., Praet, N., Kaufman, D., Haeussler, P., Loso, M. G., & De Batist, M. (2018). Varve formation during the past three centuries in three large proglacial lakes in south-Central Alaska. *Geological Society of America Bulletin*, *130*, 757–774. https://doi.org/10.1130/B31792.1

Brabets, T. P. (1993). Glacier runoff and sediment transport and deposition, Eklutna Lake basin, Alaska. *US Geological Survey Water-Resources Investigations Report*, 92–4132.

Bretherton, C. S., Widmann, M., Dymnikov, V. P., Wallace, J. M., & Bladé, I. (1999). The effective number of spatial degrees of freedom of a time-varying field. *Journal of Climate*, *12*, 1990–2009. https://doi.org/10.1175/1520-0442(1999)012%3C1990:TENOSD%3E2.0.CO;2

Burnham, K. P., & Anderson, D. R. (2002). *Model selection and multimodel inference*. Springer-Verlag. https://doi.org/10.1007/b97636

Calcagno, V., & de Mazancourt, C. (2010). Glmulti: An R package for easy automated model selection with (generalized) linear models. *Journal of Statistical Software*, *34*(12), 1–29. https://doi.org/10.18637/jss.v034.i12

Delaney, I., Bauder, A., Werder, M. A., & Farinotti, D. (2018). Regional and annual variability in subglacial sediment transport by water for two glaciers in the Swiss Alps. *Frontiers in Earth Science*, *6*, 175. https://doi.org/10.3389/feart.2018.00175

Desloges, J. R., & Gilbert, R. (1991). Sedimentary record of Harrison Lake: Implications for deglaciation in southwestern British Columbia. *Canadian Journal of Earth Sciences*, *28*, 800–815. https://doi.org/10.1139/e91-069

Ekblom Johansson, F., Bakke, J., Støren, E. N., Paasche, Ø., Engeland, K., & Arnaud, F. (2020). Lake sediments reveal large variations in flood frequency over the last 6,500 years in South-Western Norway. *Frontiers in Earth Science*, *8*, 239. https://doi.org/10.3389/feart.2020.00239

Evans, M., & Church, M. (2000). A method for error analysis of sediment yields derived from estimates of lacustrine sediment accumulation. *Earth Surface Processes and Landforms*, *25*, 1257–1267. https://doi.org/10.1002/1096-9837(200010)25:11%3C1257::AID-ESP136%3E3.0.CO;2-K

Fortin, D., Praet, N., McKay, N. P., Kaufman, D. S., Jensen, B. J., Haeussler, P. J., Buchanan, C., & De Batist, M. (2019). New approach to assessing age uncertainties–the 2300-year varve chronology from Eklutna Lake, Alaska (USA). *Quaternary Science Reviews*, *203*, 90–101. https://doi.org/10.1016/j.quascirev.2018.10.018

Fouinat, L., Sabatier, P., Poulenard, J., Etienne, D., Crouzet, C., Develle, A. L., Doyen, E., Malet, E., Reyss, J.-L., Sagot, C., Bonet, R., & Arnaud, F. (2017). One thousand seven hundred years of interaction between glacial activity and flood frequency in proglacial Lake Muzelle (western French Alps). *Quaternary Research*, *87*, 407–422. https://doi.org/10.1017/qua.2017.18

Geck, J., Hock, R., Loso, M. G., Ostman, J., & Dial, R. (2021). Modeling the impacts of climate change on mass balance and discharge of Eklutna glacier, Alaska, 1985–2019. *Journal of Glaciology*, 1–12. https://doi.org/10.1017/jog.2021.41

Gilbert, R., & Shaw, J. (1981). Sedimentation in proglacial Sunwapta Lake, Alberta. *Canadian Journal of Earth Sciences*, *18*, 81–93. https://doi.org/10.1139/e81-007

Gilli, A., Anselmetti, F. S., Glur, L., & Wirth, S. B. (2013). Lake sediments as archives of recurrence rates and intensities of past flood events. In M. Schneuwly-Bollschweiler, M. Stoffel, & F. Rudolf-Miklau (Eds.), *Dating torrential processes on fans and cones, advances in global change research* (pp. 225–242). Springer. https://doi.org/10.1007/978-94-007-4336-6

Gurnell, A. M., Clark, M. J., Hill, C. T., & Greenhalgh, J. (1992). Reliability and representativeness of a suspended sediment concentration monitoring programme for a remote alpine proglacial river. In J. Bogen, D. E. Walling, & T. Day (Eds.), *Erosion and sediment transport monitoring in river basins, proceedings of the Oslo symposium* (pp. 191–200). IAHS Press.

Hallet, B., Hunter, L., & Bogen, J. (1996). Rates of erosion and sediment evacuation by glaciers: A review of field data and their implications. *Global and Planetary Change*, *12*, 213–235. https://doi.org/10.1016/0921-8181(95)00021-6

Hamblin, P. F., & Carmack, E. C. (1978). River-induced currents in a fjord lake. *Journal of Geophysical Research: Oceans*, *83*(C2), 885–899. https://doi.org/10.1029/JC083iC02p00885

Heideman, M., Menounos, B., & Clague, J. J. (2018). A multi-century estimate of suspended sediment yield from Lillooet Lake, southern Coast

Mountains, Canada. *Canadian Journal of Earth Sciences*, *55*, 18–32. https://doi.org/10.1139/cjes-2017-0025

Hodder, K. R., Gilbert, R., & Desloges, J. R. (2007). Glaciolacustrine varved sediment as an alpine hydroclimatic proxy. *Journal of Paleolimnology*, *38*, 365–394. https://doi.org/10.1007/s10933-006-9083-9

Hodgkins, R. (1999). Controls on suspended-sediment transfer at a high-arctic glacier, determined from statistical modelling. *Earth Surface Processes and Landforms*, *24*, 1–21. https://doi.org/10.1002/(SICI)1096-9837(199901)24:1%3C1::AID-ESP936%3E3.0.CO;2-P

Jacquet, J., McCoy, S. W., Mcgrath, D., Nimick, D. A., Fahey, M., O'kuinghttons, J., & Leidich, J. (2017). Hydrologic and geomorphic changes resulting from episodic glacial lake outburst floods: Rio Colonia, Patagonia, Chile. *Geophysical Research Letters*, *44*, 854–864. https://doi.org/10.1002/2016GL071374

Kido, D., Chikita, K. A., & Hirayama, K. (2007). Subglacial drainage system changes of the Gulkana glacier, Alaska: Discharge and sediment load observations and modelling. *Hydrological Processes*, *21*, 399–410. https://doi.org/10.1002/hyp.6364

Lamke, R. D., Van Maanen, J. L., Bigelow, B. B., Still, P. J., & Kemnitz, R. T. (1990). Water resources for Alaska, water year 1989. Available from National Technical Information Service, Springfield, VA 22161 as PB 90–270620. USGS Water-Data Report AK-89-1. (USGS/WRD/HD-90/286), 1990. 224.

Lamoureux, S. F., Gilbert, R., & Lewis, T. (2002). Lacustrine sedimentary environments in high Arctic proglacial bear Lake, Devon Island, Nunavut, Canada. *Arctic, Antarctic, and Alpine Research*, *34*, 130–141. https://doi.org/10.1080/15230430.2002.12003477

Leggat, M. S., Owens, P. N., Stott, T. A., Forrester, B. J., Déry, S. J., & Menounos, B. (2015). Hydro-meteorological drivers and sources of suspended sediment flux in the pro-glacial zone of the retreating Castle Creek glacier, Cariboo Mountains, British Columbia, Canada. *Earth Surface Processes and Landforms*, *40*, 1542–1559. https://doi.org/10.1002/esp.3755

Loso, M. G. (2009). Summer temperatures during the medieval warm period and little ice age inferred from varved proglacial lake sediments in southern Alaska. *Journal of Paleolimnology*, *41*, 117–128. https://doi.org/10.1007/s10933-008-9264-9

Lunsford, A., & Rundquist, L. (2006). *August flooding in southcentral Alaska*. *Kiugmek. October Issue (pp. 1–2)* . Pacific River Forecast Center. https://www.weather.gov/media/aprfc/newsletter/fall06.pdf

Mao, L., Comiti, F., Carrillo, R., & Penna, D. (2019). Sediment transport in proglacial rivers. In *Geomorphology of proglacial systems* (pp. 199–217). Springer. https://doi.org/10.1007/978-3-319-94184-4_12

Menounos, B., & Clague, J. J. (2008). Reconstructing hydro-climatic events and glacier fluctuations over the past millennium from annually laminated sediments of Cheakamus Lake, southern Coast Mountains, British Columbia, Canada. *Quaternary Science Reviews*, *27*, 701–713. https://doi.org/10.1016/j.quascirev.2008.01.007

Menounos, B., Clague, J. J., Gilbert, R., & Slaymaker, O. (2005). Environmental reconstruction from a varve network in the southern Coast Mountains, British Columbia, Canada. *The Holocene*, *15*, 1163–1171. https://doi.org/10.1191%2F0959683605hl888rp

National Oceanic and Atmospheric Association (NOAA). (1996). *South central Alaska floods September 19–October 2, 1995. Boulder, CO, U.S. Department of Commerce*. National and Oceanic and Atmospheric Association. National Weather Service. (Flood Report). https://www.govinfo.gov/content/pkg/CZIC-gb1399-2-s68-1996/pdf/CZIC-gb1399-2-s68-1996.pdf

Ostman, J. S. (in progress). Runoff contributions to the annual water balance from two adjacent glacierized catchments with differing glacier cover, Eklutna, Alaska. (MS thesis, Alaska Pacific University, Anchorage, AK).

Ostman, J. S., Geck, J., Loso, M. G., & Larquier, A. M. (in progress). Eklutna Lake headwaters near Anchorage, Alaska: Meteorological, glacier, and fluvial system data record for 2009-2020. *Earth System Science Data*.

Praet, N., Moernaut, J., Van Daele, M., Boes, E., Haeussler, P. J., Strupler, M., Schmidt, S., Loso, M. G., & De Batist, M. (2017). Paleoseismic potential of sublacustrine landslide records in a high-seismicity setting (south-Central Alaska). *Marine Geology*, *384*, 103–119. https://doi.org/10.1016/j.margeo.2016.05.004

Praet, N., Van Daele, M., Collart, T., Moernaut, J., Vandekerkhove, E., Kempf, P., Haeussler, P. J., & De Batist, M. (2020). Turbidite stratigraphy in proglacial lakes: Deciphering trigger mechanisms using a statistical approach. *Sedimentology*, *67*, 2332–2359. https://doi.org/10.1111/sed.12703

R&M Consultants. (1986). Glacial Lake physical limnology studies: Eklutna Lake, Alaska. Susitna Hydroelectric Project Final Report No. 3070. https://www.arlis.org/docs/vol1/Susitna/30/APA3070.pdf

Rantz, S. E. (1982). Measurement and computation of streamflow. Volume 1: Measurement of stage and discharge. Volume 2: Computation of discharge. U.S. Geological Survey Water Supply Paper. 2175. https://pubs.usgs.gov/wsp/wsp2175

Richards, G., & Moore, R. D. (2003). Suspended sediment dynamics in a steep, glacier-fed mountain stream, Place Creek, Canada. *Hydrological Processes*, *17*, 1733–1753. https://doi.org/10.1002/hyp.1208

Roop, H. A., Levy, R., Dunbar, G. B., Vandergoes, M. J., Howarth, J., Fitzsimons, S., Moon, H. S., Zammit, C., Ditchburn, R., Baisden, T., & Yoon, H. I. (2016). A hydroclimate-proxy model based on sedimentary facies in an annually laminated sequence from Lake Ohau, South Island, New Zealand. *Journal of Paleolimnology*, *55*, 1–16. https://doi.org/10.1007/s10933-015-9853-3

Røthe, T. O., Bakke, J., Støren, E. W., & Bradley, R. S. (2018). Reconstructing Holocene glacier and climate fluctuations from lake sediments in Vårfluesjøen, northern Spitsbergen. *Frontiers in Earth Science*, *6*, 91. https://doi.org/10.3389/feart.2018.00091

Sass, L. C., Loso, M. G., Geck, J., Thoms, E. E., & McGrath, D. (2017). Geometry, mass balance and thinning at Eklutna glacier, Alaska: An altitude-mass-balance feedback with implications for water resources. *Journal of Glaciology*, *63*, 343–354. https://doi.org/10.1017/jog.2016.146

Schiefer, E. (2006). Depositional regimes and areal continuity of sedimentation in a montane lake basin, British Columbia, Canada. *Journal of Paleolimnology*, *35*, 617–628. https://doi.org/10.1007/s10933-005-5265-0

Schiefer, E., Kaufman, D., McKay, N., Retelle, M., Werner, A., & Roof, S. (2017). Fluvial suspended sediment yields over hours to millennia in the high Arctic at proglacial Lake Linnévatnet, Svalbard. *Earth Surface Processes and Landforms*, *43*, 482–498. https://doi.org/10.1002/esp.4264

Schiefer, E., Slaymaker, O., & Klinkenberg, B. (2001). Physiographically controlled allometry of specific sediment yield in the Canadian cordillera: A lake sediment-based approach. *Geografiska Annaler: Series A, Physical Geography*, *83*, 55–65. https://doi.org/10.1111/j.0435-3676.2001.00144.x

Schillereff, D. N., Chiverrell, R. C., Macdonald, N., & Hooke, J. M. (2014). Flood stratigraphies in lake sediments: A review. *Earth-Science Reviews*, *135*, 17–37. https://doi.org/10.1016/j.earscirev.2014.03.011

Singh, P., Haritashya, U. K., Ramasastri, K. S., & Kumar, N. (2005). Diurnal variations in discharge and suspended sediment concentration, including runoff-delaying characteristics, of the Gangotri glacier in the Garhwal Himalayas. *Hydrological Processes*, *19*, 1445–1457. https://doi.org/10.1002/hyp.5583

Sletten, K., Blikra, L. H., Ballantyne, C. K., Nesje, A., & Dahl, S. O. (2003). Holocene debris flows recognized in a lacustrine sedimentary succession: Sedimentology, chronostratigraphy and cause of triggering. *The Holocene*, *13*, 907–920. https://doi.org/10.1191%2F0959683603hl673rp

Smith, N. D. (1978). Sedimentation processes and patterns in a glacier-fed lake with low sediment input. *Canadian Journal of Earth Sciences*, *15*, 741–756. https://doi.org/10.1139/e78-081

Smith, N. D., & Ashley, G. (1985). Proglacial lacustrine environment. In G. M. Ashley, J. Shaw, & N. D. Smith (Eds.), *Glacial sedimentary environments* (Vol. 16, pp. 135–216). SEPM, Short Course Notes.

Van Daele, M., Haeussler, P. J., Witter, R. C., Praet, N., & De Batist, M. (2020). The sedimentary record of the 2018 Anchorage earthquake in Eklutna Lake, Alaska: Calibrating the lacustrine seismograph. *Seismological Research Letters*, *91*, 126–141. https://doi.org/10.1785/0220190204

Vandekerkhove, E., Van Daele, M., Praet, N., Cnudde, V., Haeussler, P. J., & De Batist, M. (2020). Flood-triggered versus earthquake-triggered turbidites: A sedimentological study in clastic Lake sediments (Eklutna lake, Alaska). *Sedimentology*, *67*, 364–389. https://doi.org/10.1111/sed.12646

Wells, M. G. (2009). How Coriolis forces can limit the spatial extent of sediment deposition of a large-scale turbidity current. *Sedimentary Geology*, *218*, 1–5. https://doi.org/10.1016/j.sedgeo.2009.04.011

Wilhelm, B., Nomade, J., Crouzet, C., Litty, C., Sabatier, P., Belle, S., Rolland, Y., Revel, M., Courboulex, F., Arnaud, F., & Anselmetti, F. S. (2016). Quantified sensitivity of small lake sediments to record historic earthquakes: Implications for paleoseismology. *Journal of Geophysical Research: Earth Surface*, *121*, 2–16. https://doi.org/10.1002/2015JF003644

Williams, G. P. (1989). Sediment concentration versus water discharge during single hydrologic events in rivers. *Journal of Hydrology*, *111*, 89–106. https://doi.org/10.1016/0022-1694(89)90254-0

Wilson, F. H., & Hults, C. P. (2012). Geology of the Prince William sound and Kenai peninsula region, Alaska. *US Geological Survey Scientific Investigations Map*, 3110–37. https://doi.org/10.3133/sim3110

How to cite this article: Schiefer, E., Geck, J., Ostman, J. S., McKay, N. P., Praet, N., Loso, M. G., & Kaufman, D. S. (2021). Fluvial suspended sediment transfer and lacustrine sedimentation of recent flood turbidites in proglacial Eklutna Lake, western Chugach Mountains, Alaska. *Hydrological Processes*, *35*(10), e14375. https://doi.org/10.1002/hyp.14375